Experimental study on pore structure evolution of thermally treated shales: implications for CO2 storage in underground thermally treated shale horizons

Hazra, Bodhisatwa; Chandra, Debanjan; Vishal, Vikram; Ostadhassan, Mehdi; Sethi, Chinmay; Saikia, Binoy K.; Pandey, Jai Krishna; Varma, Atul K.

DOI
10.1007/s40789-024-00717-6

Publication date
2024

Document Version
Final published version

Published in
International Journal of Coal Science and Technology

Citation (APA)
Hazra, B., Chandra, D., Vishal, V., Ostadhassan, M., Sethi, C., Saikia, B. K., Pandey, J. K., & Varma, A. K. (2024). Experimental study on pore structure evolution of thermally treated shales: implications for CO2 storage in underground thermally treated shale horizons. *International Journal of Coal Science and Technology*, *11*(1), Article 61. https://doi.org/10.1007/s40789-024-00717-6

International Journal of Coal Science & Technology (2024) 11:61
https://doi.org/10.1007/s40789-024-00717-6

RESEARCH

Experimental study on pore structure evolution of thermally treated shales: implications for CO_2 storage in underground thermally treated shale horizons

Bodhisatwa Hazra[1,2] · Debanjan Chandra[3] · Vikram Vishal[4,5] · Mehdi Ostadhassan[2] · Chinmay Sethi[1] · Binoy K. Saikia[6] · Jai Krishna Pandey[1] · Atul K. Varma[7]

Received: 31 December 2023 / Revised: 18 March 2024 / Accepted: 14 June 2024

Abstract

Extracting gas from unconventional shale reservoirs with low permeability is challenging. To overcome this, hydraulic fracturing (HF) is employed. Despite enhancing shale gas production, HF has drawbacks like groundwater pollution and induced earthquakes. Such issues highlight the need for ongoing exploration of novel shale gas extraction methods such as in situ heating through combustion or pyrolysis to mitigate operational and environmental concerns. In this study, thermally immature shales of contrasting organic richness from Rajmahal Basin of India were heated to different temperatures (pyrolysis at 350, 500 and 650 °C) to assess the temperature protocols necessary for hydrocarbon liberation and investigate the evolution of pore structural facets with implications for CO_2 sequestration in underground thermally treated shale horizons. Our results from low-pressure N_2 adsorption reveal reduced adsorption capacity in the shale splits treated at 350 and 500 ºC, which can be attributed to structural reworking of the organic matter within the samples leading to formation of complex pore structures that limits the access of nitrogen at low experimental temperatures. Consequently, for both the studied samples BET SSA decreased by ∼58% and 72% at 350 °C, and ∼67% and 68% at 500 °C, whereas average pore diameter increased by ∼45% and 91% at 350 °C, and ∼100% and 94% at 500 °C compared to their untreated counterparts. CO_2 adsorption results, unlike N_2, revealed a pronounced rise in micropore properties (surface area and volume) at 500 and 650 ºC (∼30%–35% and ∼41%–63%, respectively for both samples), contradicting the N_2 adsorption outcomes. Scanning electron microscope (SEM) images complemented the findings, showing pore structures evolving from microcracks to collapsed pores with increasing thermal treatment. Analysis of the SEM images of both samples revealed a notable increase in average pore width (short axis): by ∼4 and 10 times at 350 °C, ∼5 and 12 times at 500 °C, and ∼10 and 28 times at 650 °C compared to the untreated samples. Rock-Eval analysis demonstrated the liberation of almost all pyrolyzable kerogen components in the shales heated to 650 °C. Additionally, the maximum micropore capacity, identified from CO_2 gas adsorption analysis, indicated 650 °C as the ideal temperature for in situ conversion and CO_2 sequestration. Nevertheless, project viability hinges on assessing other relevant aspects of shale gas development such as geomechanical stability and supercritical CO_2 interactions in addition to thermal treatment.

Highlights

Insitu thermal treatment of shales for liberation of hydrocarbons and CO_2 sequestration.
Significant changes in shale geochemistry and pore properties with increasing temperatures of treatment.
Visualizing thermally induced pore evolution in shale: microcracks to collapsed pores.
Limitations of N_2 in accessing complex pore structures.

Keywords Shale · Pore structures · Microstructure · Pyrolysis · Low pressure gas adsorption analysis

Extended author information available on the last page of the article

Published online: 12 July 2024

1 Introduction

Owing to their substantial reserves and the gradual exhaustion of conventional petroleum resources, in the past few decades there has been an interest in unconventional shale reservoirs as they represent large resources, cleaner energy option, and are seen as potential targets for CO_2 sequestration and thereby a potential bridge toward the transition to renewable energy resources (Jarvie et al. 2007; Godec et al. 2013; Heller and Zoback 2014; Hazra et al. 2018b, 2022; Du and Nojabaei 2019; Lyu et al. 2021; Chandra et al. 2022, 2023). Shale reservoirs commonly exhibit extremely low permeability (10^{-1} to 10^{-4} mD) (Wang et al. 2017; Vishal et al. 2019; Xu et al. 2023), making the extraction of shale gas from these reservoirs challenging through conventional methods. However, development of extraction technologies, specifically hydraulic fracturing (HF) has resulted in unprecedented development of shale gas exploitation in the past decade (Xu et al. 2023). Despite its substantial contribution to enhancing shale gas production, the hydraulic fracturing (HF) technique is not without drawbacks, including the potential for groundwater pollution and the risk of inducing earthquakes (Bao and Eaton 2016). Moreover, HF leads to extensive water penetration and pore space trapping (Liu et al. 2020). It is crucial to continuously explore novel methods for the extraction of shale gas. In-situ heating technique such as oil shale retorting is used as alternate to HF for extraction of shale oil/gas (Liu et al. 2020). The technique of in-situ oil shale retorting, dating back to the 1970s (Krumm 2014), involves drilling wells directly into the deposit from the ground. Additional heat, such as electrical heating, is applied within the formation to facilitate in-situ rectification of oil (Kang et al. 2020).

Several studies have explored methods to improve hydrocarbon recovery from gas shales through thermal treatments, including techniques such as in-situ combustion and pyrolysis (Chaprio and Bruining, 2015; Chen et al. 2016, 2018; Chandra et al. 2021, 2023; Hazra et al. 2023). Combustion or pyrolysis induces structural changes in kerogen, leading to the regeneration and reopening of pre-existing micro- and mesopores (Kang et al. 2020; Chandra et al. 2021, 2023; Hazra et al. 2023). This process enhances effective porosity, consequently improving hydrocarbon flow within the matrix. While the effects of pyrolysis on oil shales and its consequences for in-situ thermal treatment-based oil recovery have been widely studied (Tiwari et al. 2013; Sun et al. 2015; Bai et al. 2017; Lei et al. 2021; Taheri-Shakib and Kantzas 2021; Guo et al. 2022; Shi et al. 2023), there has been limited attention to its impact on gas shales and the consequent implications for in-situ thermal treatment-based hydrocarbon recovery.

Recently, a new subsurface thermal treatment technique, known as underground coal thermal treatment (UCTT) has emerged for stimulating deeply buried coals to produce lighter hydrocarbons (Krumm 2014; Kelly et al. 2016; Zhang et al. 2017; Shi et al. 2022). In this method, energy is applied to heat the coal seam through pyrolysis, and the resulting decomposition products are collected as gaseous and liquid fuels. A significant portion of the carbon remains below the surface, creating a carbon matrix, which can additionally be targeted for CO_2 sequestration (Krumm 2014; Shi et al. 2022). Compared to underground coal gasification (UCG), UCTT has a number of advantages due to the non-oxidizing environment. Additionally, pyrolytic semi-coke or the coal char produced by UCTT serves as good storage vehicle for CO_2 geological storage (Shi et al. 2022). Similar application on organic-rich shale horizons could also become a viable method for recovery of lighter hydrocarbons and creating an in-situ shale-char with higher surface areas, which can be conducive to CO_2 storage. Several laboratory scale experimental studies have shown the impact of heat treatment on shale petrophysical properties with implications for gas recovery and storage (Chen et al. 2017, 2018; Li et al. 2022; Chandra et al. 2021, 2023; Zhang et al. 2023; Zhuoke et al. 2023). Chen et al. (2017) conducted oxic heating of thermally matured shale samples, and observed removal of organic pores at temperatures of 400–500 °C. Chen et al. (2018) observed a reduction in surface area and an increase in the mean diameter of pores in shale samples subjected to oxic heating at 500 °C. Li et al. (2022) observed that with increasing thermal treatment temperatures, there was a continuous increase in the total pore volume, quantity, and ratio of mesopores and macropores in Longmaxi shale samples. Chandra et al. (2021) conducted both oxic and anoxic heating on Permian shale samples of Raniganj basin and witnessed a notable rise in surface area and pore volume during oxic heating, while anoxic heating led to a significant reduction in these parameters. Similar observations were reported by Chandra et al. (2023) while also highlighting the augmentation of surface area and pore volume through thermal treatment enhances the feasibility of long-term CO_2 storage in shale formations. Zhang et al. (2023) found that the Brunauer–Emmett–Teller specific surface area (BET SSA) of Bohai Bay basin shale samples initially decreased, then increased, and finally decreased again as temperature rose from 110 to 500 °C. In contrast, the average pore diameter demonstrated the opposite trend. Zhuoke et al. (2023) studied the effect of total organic carbon (TOC) on evolution of pore system in immature shale samples after heat treatment and observed that higher organic content correlates with increased hydrocarbon expulsion strength and pore volume growth. The pores exhibited pronounced fractal characteristics, with fractal dimension ranging between

2.397 and 2.636, indicating extremely small and complex pore structures with strong heterogeneity. Hazra et al. (2023) studied the impact of oxic heating (at 325, 425, and 525 °C) on the evolution of pore structures in the shale samples of contrasting thermal maturities. They observed that thermal treatment at higher temperatures significantly altered mesopore and micropore structures in shales.

In this study, two shale samples, with contrasting organic richness (TOC: 16.46 wt% and 28.98 wt%) collected from the depth intervals of 426-426.40 and 580–580.90 m, of a borehole drilled at Surni Coal Block of Rajmahal Coalfield, Jharkhand, India) belonging to the Lower Permian (Epoch-Cisularian; Stage: Kungurian) Barakar Formation from Rajmahal basin, India, are thermally treated (pyrolysis) at different temperatures to determine the temperature protocols needed for liberating hydrocarbons from the shales, and additionally explore the evolution of pore structural facets due to thermal treatment for CO_2 sequestration. In general, shales from Rajmahal are thermally immature (equivalent to sub-bituminous coal rank; Sethi et al. 2023) and hence presents the opportunity to thermally stimulate them to extract cleaner hydrocarbons and create sites for CO_2 sequestration. Examining thermally immature shale and its thermally treated counterparts also allow discerning the changes in the geochemical and pore properties as shale progresses towards maturity. Our results indicate that when the samples were heated at elevated temperatures for 30 min, the hydrocarbons are liberated from the kerogen, resulting in substantial increase in micropore surface area and volume of the samples, implying an increased CO_2 sequestration potential in thermally stimulated shales.

2 Materials and methods

2.1 Sample types and thermal treatment

Two organic-rich shale samples belonging to the Lower Permian Barakar Formation from Rajmahal basin, India were selected for this study. The shales were controlled-crushed using pastel and mortar to achieve 212 microns size, which were then thermally treated, after removing a small aliquot representing the original sample. For thermal treatment, the samples were loaded in stainless steel containers, with openings in the lid, and treated in a tubular furnace, with nitrogen gas flow to maintain inert conditions. The samples were heated at temperatures of 350, 500 and 650 °C for 30 min. The raw samples (untreated aliquots) are denoted as X-RT and Y-RT, while the splits thermally treated at 350, 500 and 650 °C for 30 min are labelled as X-350/Y-350, X-500/Y-500, and X-650/Y-650, respectively.

2.2 Rock-eval

Rock-Eval 6, manufactured by Vinci Technologies was used to analyse the hydrocarbon generation properties of the raw shales and the thermally treated splits. A modified version of Rock-Eval's "basic/bulk-rock method" was used to analyse the samples, with 750 °C set as the final oxidation temperature. This approach followed the protocols developed by Hazra et al. (2017, 2019) to ensure reliable data generation for Type III-IV kerogen rich samples.

2.3 Low pressure gas adsorption

Low pressure gas adsorption (LPGA) analysis of the raw shale samples (X-RT and Y-RT), and its thermally treated counterparts (X-350/Y-350, X-500/Y-500, and X-650/Y-650) was conducted for evaluation for their pore structure characteristics, including surface area, pore volume, and size distribution. Samples crushed to 212 microns were used for conducting the experiments. Additionally, prior to conducting the experiments, the samples were subjected to degassing for 3 h at 110 °C (Hazra et al. 2018a; Singh et al. 2021). Quantachrome® Autosorb iQ apparatus was used for the analysis with Nitrogen (N_2) and carbon dioxide (CO_2) used as adsorbates. The relative pressure of the adsorbate (P/P_0) was increased steadily over the course of LPGA investigation until it reached the condensation pressure that is unique to the adsorbate's temperature. In this case, P_0 represents the adsorbate's condensation pressure, and P represents the saturation pressure at each pressure point. The LPGA experiment using N_2 was carried out at 77 K temperature and 1 bar of saturation pressure. A comprehensive set of 40 data points was recorded across the pressure ratio (P/P_0) spectrum, ranging from 0.01 to 0.99. The experiments involving LPGA using CO_2 were executed under precisely controlled conditions within a water bath sustained at a consistent temperature of 273 K. The experiments included P/P_0 values between 0.0005 and 0.03. Nitrogen (N_2) isotherms were also utilised to assess the Barret-Joyner-Halenda (BJH), pore size distribution (PSD), Brunauer, Emmett and Teller (BET) specific surface area (SSA) and Frenkel-Halsey-Hill (FHH) fractal dimensions. The specific surface area was determined using the multipoint BET equation. Through linearization of the BET equation, the slope and intercept reveal monolayer adsorption behavior, facilitating precise calculations of surface area based on the nitrogen monolayer adsorption volume and molecular weight. The Barret-Joyner-Halenda (BJH) model was used to calculate pore size distribution from nitrogen desorption isotherms (Barrett et al. 1951). Utilizing the Kelvin equation (Pirngruber 2016), it relates pore size to relative pressure, deriving differential pore volume and

providing insights into the distribution of pore sizes within the shale. The micropores surface area was determined from CO_2 adsorption isotherms using the Dubinin-Radushkevich (DA) equation (Dabrowski 2001). Graphical analysis such as plotting ln(Q) against ε^2, where Q represents adsorbed gas, and ε signifies Polanyi potential, provides the value of β (adsorption potential). The micropore surface (S_{micro}) area was then calculated applying the equation:

$$S_{\text{micro}} = \frac{1}{4}\pi\beta^2 \tag{1}$$

The Dubinin-Astakhov (DA) method was used to calculate the micropore volume from the equation (Günay et al. 2007):

$$V_{\text{mic}} = \frac{V_0}{2}\int_0^{\ln\left(\frac{P}{P_0}\right)} e^{\beta E^2}\text{dln}(\text{P}/\text{P}_0) \tag{2}$$

Where, V_0 is a material constant, β is the adsorption potential, E is the characteristic energy of adsorption, and P/P_0 relative pressure. The integration over the natural logarithm of the pressure ratio, derived from adsorption isotherm data yields micropore volume. The density functional theory (DFT) method was used to assess the micropore size distribution (Thommes et al. 2015). The foundation of the DFT model lies in utilizing molecular statistical thermodynamics to determine the specific adsorption quantity within a defined pore range at a given experimental temperature and pressure. This is achieved by solving the equation for grand thermodynamic potential, which is intricately linked to the distribution of gas density within a specific pore space.

The low pressure N_2 gas adsorption data was used to calculate fractal dimensions of the shales and their thermally treated counterparts following the Frenkel-Halsey-Hill (FHH) adsorption isotherm equation (reference). The FHH technique requires the construction of the lnN versus ln(-lnX) graphic using the N_2 adsorption isotherm data, where X denotes P/P_0. The slope of a straight line fitted to that data trend is used to calculate the fractal dimension (D) applying Eq. (3)

$$InN = a + (D-3) * \ln(-\text{lnX}) \tag{3}$$

Where, a is a constant and (D-3) is the slope of the best-fit line.

Ideally, two specific fractal dimensions are typically distinguished: (1) D1 (surface fractal dimension, calculated at the lower relative pressure range where the nature of adsorption is contemplated to be governed by van der Waals forces); and, (2) D2 (pore structural fractal dimension calculated at higher relative pressure range where the nature of adsorption is governed by capillary condensation (Khalili et al. 2000; Yao et al. 2008).

2.4 Field emission scanning electron microscopy

The two shale samples (X-RT and Y-RT) and their thermally treated counterparts (X-350/Y-350, X-500/Y-500, and X-650/Y-650) of 212 microns size after heating were gold coated for a duration of 2 min before being introduced into the Carl Zeiss Merlin VP Compact field emission scanning electron microscope (FE-SEM). Sample analysis was conducted using both Secondary Electron (SE2) and Angle Selective Backscattered (AsB) modes. The primary objective of this analysis was to discern and comprehend the structural alterations within the thermally treated shale samples in direct comparison to their untreated counterparts.

3 Results and discussion

3.1 Changes in thermal maturity with increasing temperatures of treatment

Table 1 presents the results of the two shales (X-RT and Y-RT) and their thermally treated counterparts. For the raw shales, X-RT and Y-RT, T_{max} of the samples can be observed to be 430 and 429 °C, respectively, indicating them to be thermally immature (Peters and Cassa 1994). For these two samples, the S2 was found to be 17.89 and 24.27 mg HC/g rock, respectively. With increasing temperatures of treatment, the S2 of the samples systematically decreased,

Table 1 Source rock properties of the raw and thermally treated shale samples

No.	S1 (mg HC/g rock)	S2 (mg HC/g rock)	T_{max} (°C)	S3 (mg CO_2/g rock)	PC (wt%)	RC (wt%)	TOC (wt%)	HI (mg HC/g TOC)	OI (mg CO2/g TOC)	S4 T_{peak} (ºC)
X-RT	0.10	17.89	430	3.17	1.75	14.71	16.46	109	19	471
X-350	0.14	8.64	458	1.86	0.96	14.51	15.47	56	12	477
X-500	0.58	0.62	605	1.09	0.18	14.01	14.19	4	8	500
X-650	0.14	0.08	258	1.07	0.07	13.69	13.76	1	8	555
Y-RT	0.10	24.47	429	1.86	2.27	26.71	28.98	84	6	504
Y-350	0.19	3.49	554	1.60	0.50	26.08	26.58	13	6	509
Y-500	0.18	0.29	606	0.99	0.10	25.19	25.29	1	4	516
Y-650	0.20	0.26	302	0.97	0.09	23.25	23.34	1	4	558

which is caused due to expulsion of hydrocarbons from the samples. Figures 1 and 2 shows the S2 curves of the two shales and their thermally treated splits. While for the raw shales and the splits treated at 350 °C (Figs. 1a and 2a), the S2 curves (and T_{max}) were observed to be reliable, for the splits treated at 500 and 650 °C (Figs. 1b and 2b), the nature of the S2 curves can be seen to be highly irregular and consequently the T_{max} calculated from these S2 curves are unreliable. This phenomenon primarily occurs as a result of the systematic expulsion of greater amounts of hydrocarbons from the samples with increasing temperatures of treatment.

For heat-altered and low-TOC shales, characterized by irregular S2 curves and consequently unreliable T_{max}, Hazra et al. (2021) have recently introduced Rock-Eval S4T_{peak} as proxy for thermal maturity. The S4T_{peak} is calculated from the temperature peak observed in the S4CO_2 curve, generated during the Rock-Eval oxidation stage. For both the shales, with increasing temperatures of thermal treatment, the S4T_{peak} was observed to increase (Fig. 3). This indicates

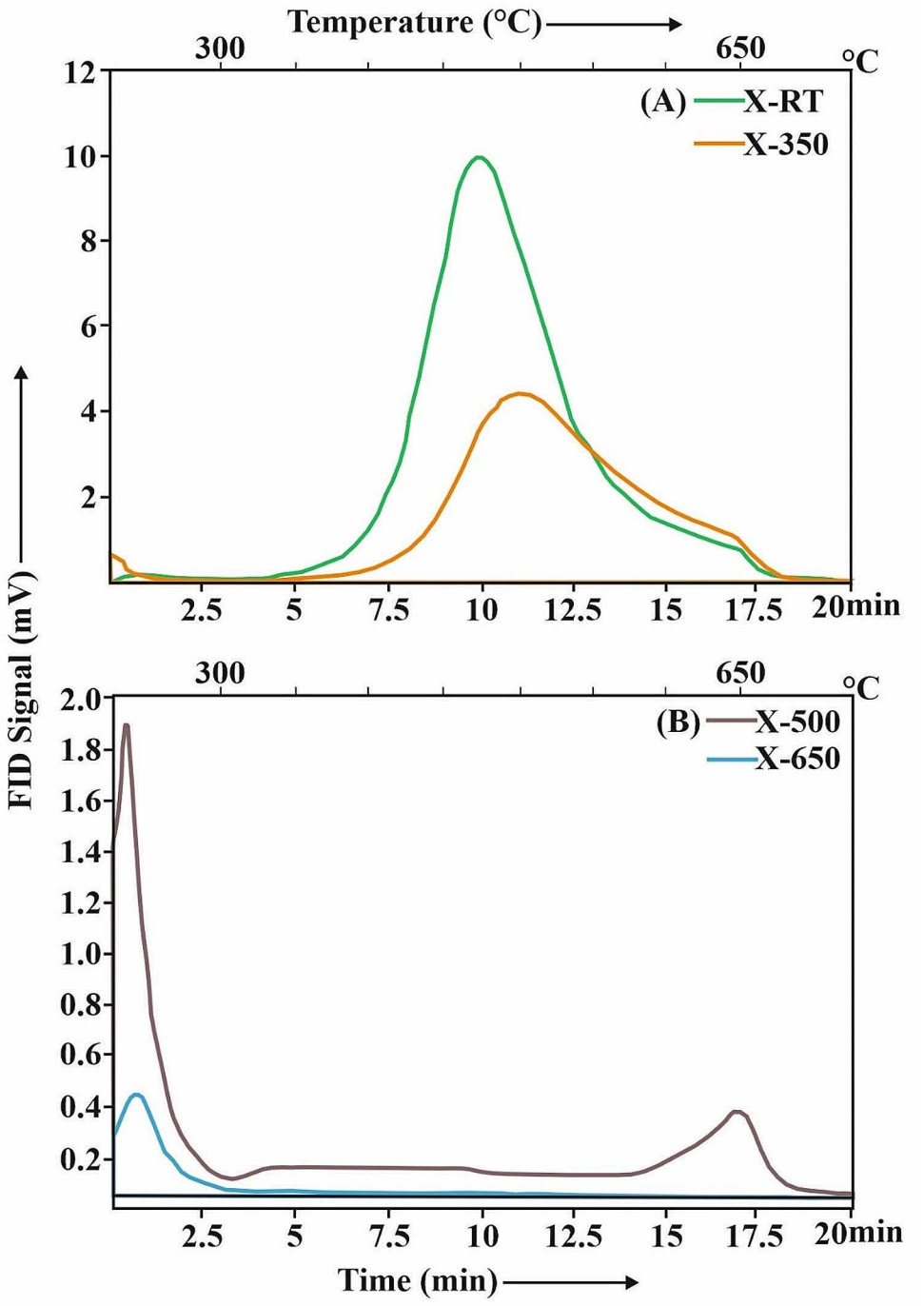

Fig. 1 S2 pyrograms of sample X-RT and its thermally treated counterparts: **a** X-RT and X-350 **b** X-500 and X-650

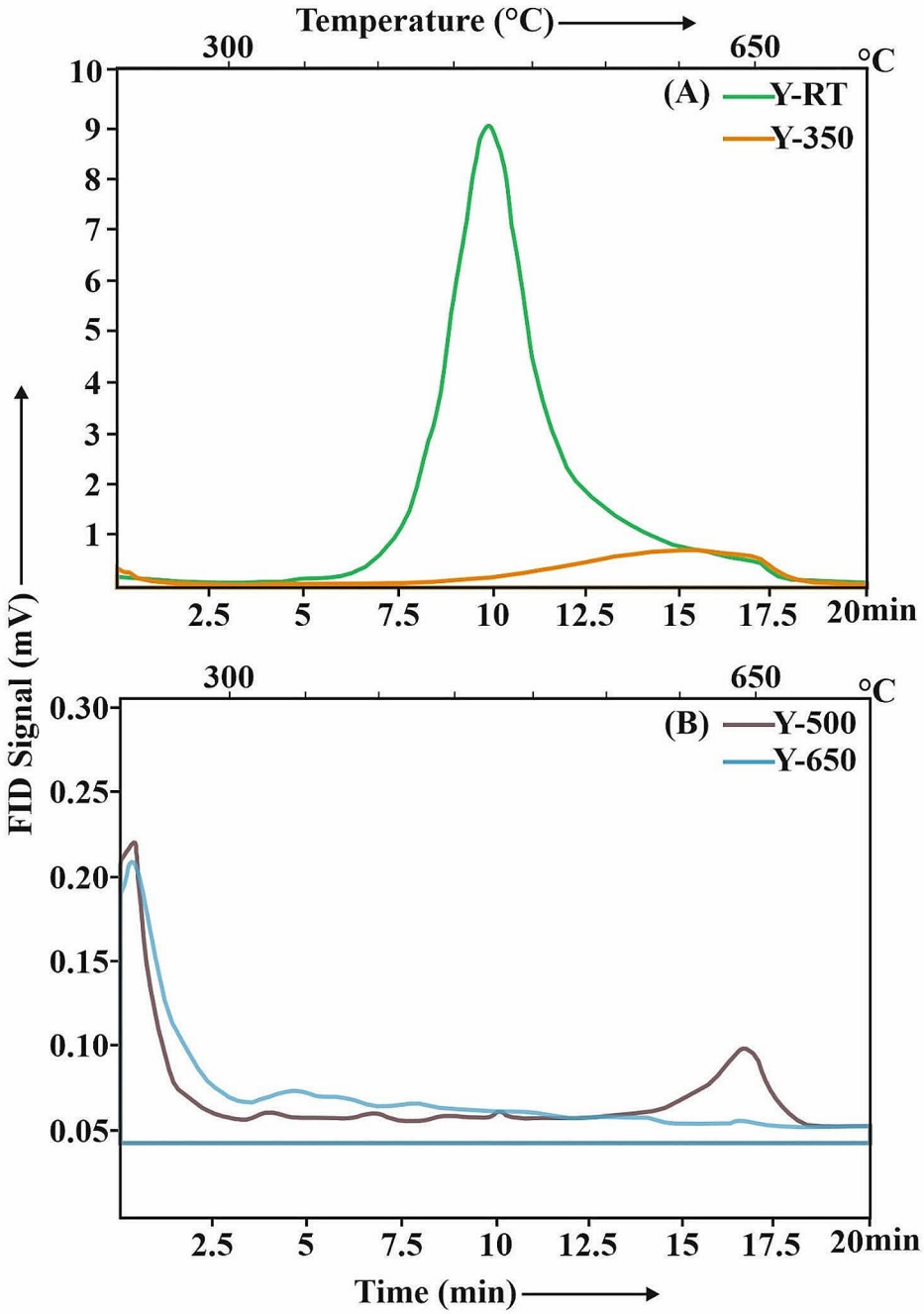

Fig. 2 S2 pyrograms of sample Y-RT and its thermally treated counterparts: **a** Y-RT and Y-350 **b** Y-500 and Y-650

that with increasing temperatures of thermal treatment, as hydrocarbons are expelled from the samples, the remaining organic matter within the shales become more and more aromatized, and thereby requiring higher temperatures to react/crack and generate CO_2/CO during oxidation. The results also further substantiate the usage of Rock-Eval S4T_{peak} as a thermal maturity proxy, especially applicable for low-TOC and heat-altered shales where T_{max} from pyrolysis stage is less reliable. It can be effectively summarized from the Rock-Eval results that with increasing temperatures of treatment, hydrocarbons are systematically removed from the samples signified by lowering of S2 and PC, and the resultant shale-chars successively requiring higher temperatures (i.e., higher S4T_{peak}) during oxidation to decompose.

One of the main advantages often cited for in situ thermal treatment of coal seams (under inert conditions) in comparison to underground coal gasification is the potential for extracting only lighter hydrocarbons, leaving a significant amount of carbon as char and creation of microporous structures in situ, which can subsequently be used for sequestrating CO_2 (Shi et al. 2022). Rock-Eval results from the thermally treated splits of the shales clearly substantiates

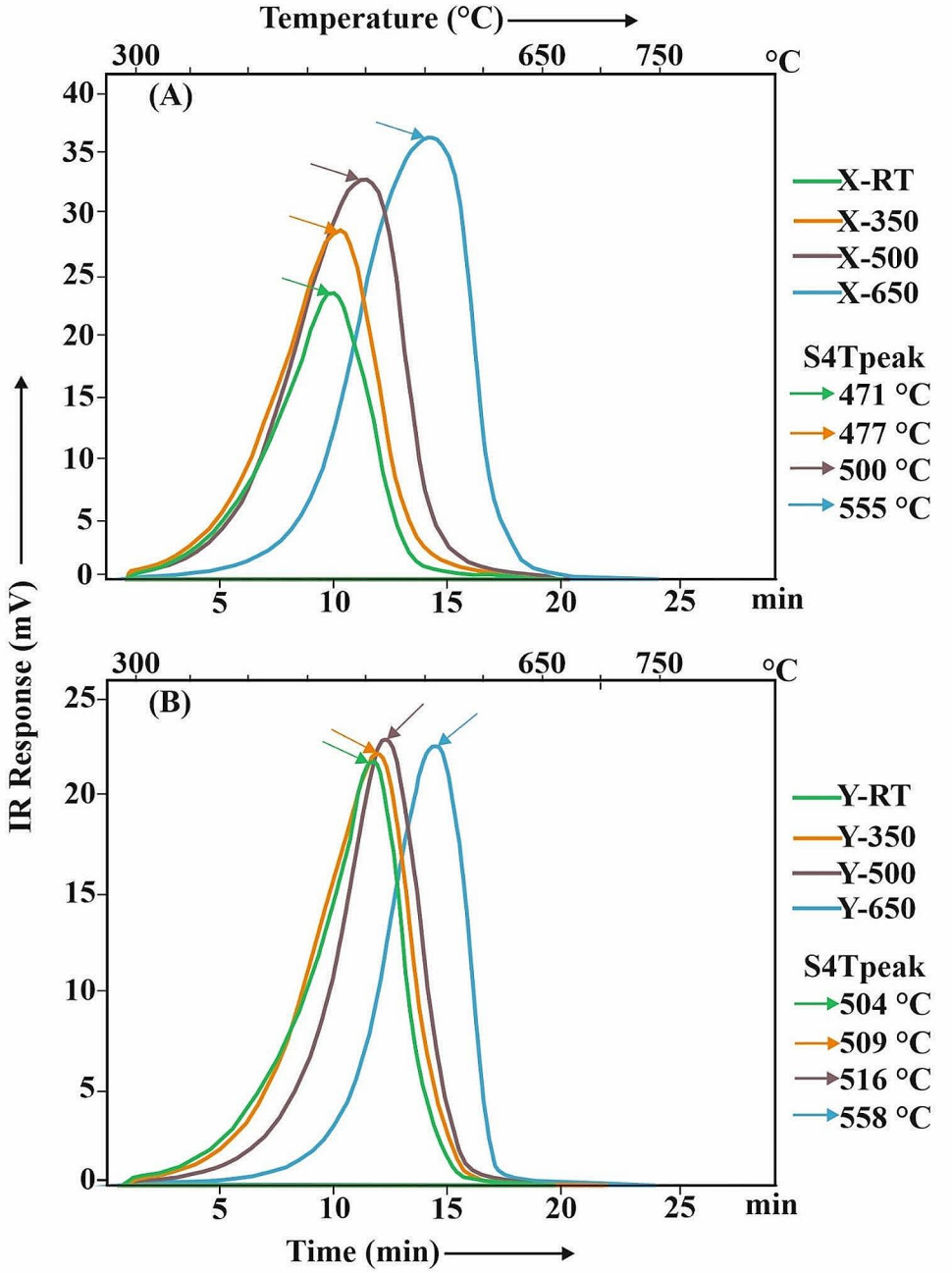

Fig. 3 $S4CO_2$ oxidation graphics of sample **a** X-RT and **b** Y-RT along with their thermally treated counterparts, including corresponding $S4T_{peak}$ values at different thermal treatment temperatures

that with increasing temperatures of treatment, the pyrolyzable carbon (PC) is significantly reduced due to liberation and removal of hydrocarbons. On the other hand, the residual carbon (RC) of the thermally treated splits are substantially high (albeit some reduction with increasing temperatures), indicating that significant portion of the carbon exists within the shale-char created from thermal treatment. The increasing $S4T_{peak}$ from the oxidation stage of Rock-Eval also indicates the aromatization of the samples and formation of successively more aromatized shale-char owing to thermal treatment. The shale-char generated in situ through thermal treatment, may thus offer additional sites for storage of injected CO_2.

3.2 Inferences from low pressure N_2 gas adsorption

3.2.1 Pore structural parameters

Figures 4 and 5 plots the low-pressure nitrogen gas adsorption isotherms of the raw shale samples, and its thermally treated counterparts. For the two raw shales X-RT and Y-RT used in this study, the nitrogen gas adsorption derived BET

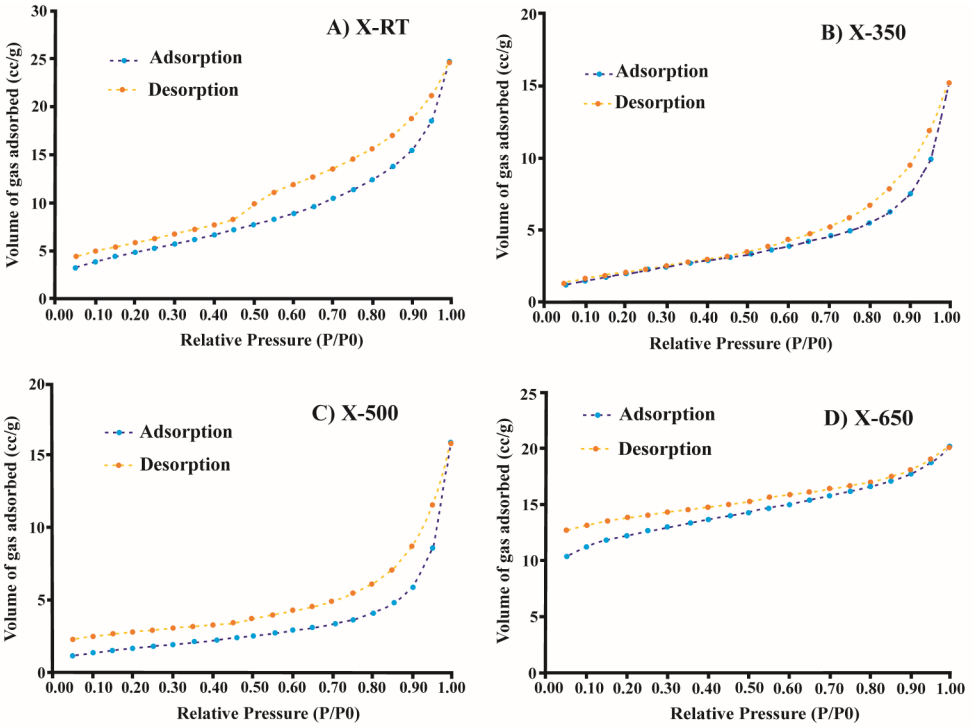

Fig. 4 Adsorption and desorption isotherms of **a** X-RT shale and its thermally treated counterparts: **b** X-350, **c** X-500, and **d** X-650, obtained from LPGA analysis using nitrogen gas

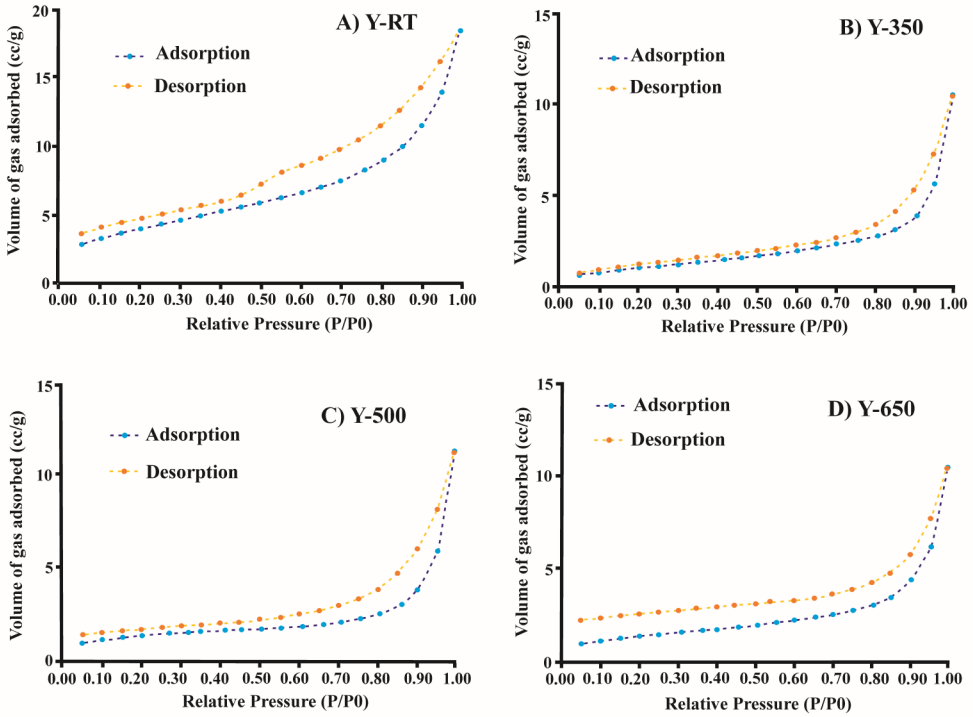

Fig. 5 Adsorption and desorption isotherms of **a** Y-RT shale and its thermally treated counterparts: **b** Y-350, **c** Y-500, and **d** Y-650, obtained from LPGA analysis using nitrogen gas

SSA was observed to be 18.46 and 14.57 m^2/g, with average pore radius being 8.26 and 7.78 nm, respectively.

The shape of the low pressure nitrogen gas adsorption isotherm reflects the type of pore present within the samples (Kuila and Prasad, 2013). The IUPAC classifies adsorption isotherms into 6 types and a detailed description of the classification of isotherms can be found in Sing (1985) and Rouquerol et al. (1998). For both the samples (Figs. 4 and 5), significant hysteresis was observed, implying occurrence of capillary condensation within the mesopores (Sing, 1985). However, none of the isotherms show any development of a plateau at the highest relative pressures, which is

Table 2 Pore structural parameters obtained through Low-pressure N_2 gas adsorption

No.	BET SSA (m^2/g)	BJH pore volume (cc/g)	Average pore diameter (nm)	Fractal dimension D1	Fractal dimension D2
X-RT	18.458	0.034	8.26	2.40	2.75
X-350	7.816	0.022	11.98	2.24	2.67
X-500	6.177	0.023	15.81	2.44	2.61
X-650	38.383	0.014	3.25	2.78	2.93
Y-RT	14.572	0.024	7.78	2.50	2.79
Y-350	4.122	0.016	15.68	2.34	2.63
Y-500	4.608	0.016	15.09	2.56	2.59
Y-650	4.84	0.015	13.27	2.50	2.63

typical of type IV isotherms for mesoporous materials, with the plateau implying completion of mesopore filling (Kuila and Prasad, 2013; Hazra et al. 2018a). Rather the isotherms show development of steep slopes at the highest relative pressures, implying presence of macropores (Kuila and Prasad, 2013; Hazra et al. 2018a). Rouquerol et al. (1998) designated such isotherms as Type IIB i.e., samples marked by presence of both mesopores (causing hysteresis) and macropores (causing absence of plateau like those shown by Type IV materials). Consequently, the adsorption isotherms for the studied samples are identified as Type IIb (Figs. 4 and 5). The shape of the pores is inferred indirectly through the analysis of the N_2 adsorption isotherm, particularly focusing on the slope and curvature of the adsorption branches. The hysteresis loops in the desorption branch can indicate the pore shapes. De Boer (1958) classifies hysteresis loops into five types, each correlated with distinct pore shapes. Specifically, Type A hysteresis is linked to cylindrical pores, Type B to slit-shaped pores, Types C and D hysteresis are indicative of wedge-shaped pores, and Type E associated with bottle neck pores (Labani et al. 2013). Both shale samples exhibit Type B hysteresis loops (Figs. 4 and 5), suggesting the prevalence of predominantly slit-shaped pores.

As the thermal treatment temperatures increased, marked changes in the adsorption isotherm characteristics were observed for both the samples. Compared to the raw samples, the X-350 and Y-350 splits exhibited a significant reduction in adsorption capacity at the lowest experimental pressures. A similar reduction in adsorption capacity was also observed for the X-500 and Y-500 splits at the lowest experimental pressures. What this essentially indicates is that due to thermal treatment at 350 and 500 ºC, as the organic matter within the shales react and generate hydrocarbons, some structural reworking within the samples take place, which limits the entry of nitrogen in assessing the finer mesopore structures. On the other hand, for the sample splits thermally treated at 350 and 500 ºC, tightening of the hysteresis loops was noted, which indicates that the connectivity of coarser mesopores is improved during hydrocarbon generation due to thermal treatment. Consequently, a decrease in BET SSA and an increase in the average pore radius was observed for splits treated at 350 and 500 °C (Table 2).

The restricted entry of N2 into the pore spaces of the splits treated at 350 and 500 ºC is also manifested in the BJH pore size distribution (PSD) plot. Notably, for the X-350, X-500, Y-350 and Y-500 splits, the volume of pores in the smaller sizes (~10 nm) is several times smaller compared to their respective raw splits (Fig. 6). Interestingly, compared to the raw sample and the other splits, for the

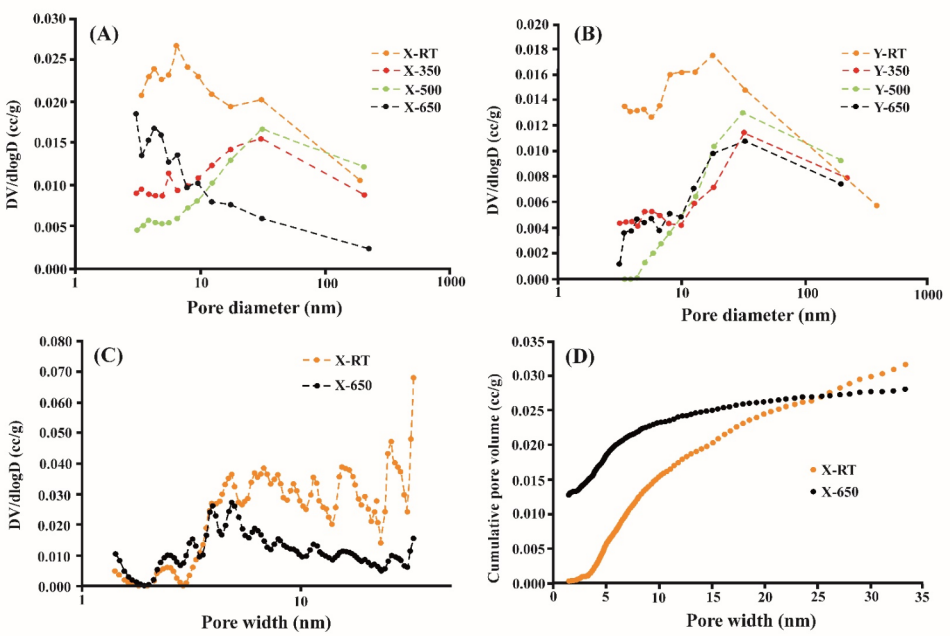

Fig. 6 PSD plots for sample **a** X-RT and its thermally treated counterparts, and for **b** Y-RT and its thermally treated counterparts derived using BJH adsorption model **c** PSD plots of sample X-RT and **d** its thermally treated X-650 split derived using the DFT model

X-650 split the BET SSA was observed to sharply increase (38.38 m^2/g; even higher than X-RT), with the average pore radius being sharply reduced (3.25 nm; even lower than that of X-RT). However, for sample Y-650, BET SSA (4.84 m^2/g) was observed to only marginally increase compared to Y-500 (4.61 m^2/g), and thereby being much lower than Y-RT. Similarly, for the Y-650 split average pore radius was observed to be marginally lower compared to the Y-500 and Y-350 splits, but much larger than the Y-RT split. Careful consideration of the Rock-Eval data also shows contrasting behaviour of the two shales, despite of them having similar HI and thermal maturity levels (Table 1). S1 was first observed to increase from 0.10 mg HC/g rock (for X-RT) to 0.14 mg HC/g rock (for split X-350), followed by a sharp increase for the X-500 split (0.58 mg HC/g rock), followed by a sharp decrease for the X-650 split (0.14 mg HC/g rock). The sharp increase in S1 for the X-500 split could be due to generation of greater amounts of free hydrocarbons from the organic matter within the sample caused due to higher temperature thermal treatment. With further thermal stimulation (650 ºC), substantial portion of the free hydrocarbons are expelled from the sample. In contrast for sample Y-RT and the other splits, no sharp increase or decrease in S1 was noted, with near similar S1 for the Y-350, Y-500 and Y-650 splits but higher than the Y-RT split. While the BJH PSD plot shows opening of larger number of smaller mesopores in X-650, relative to X-350 and X-500 splits, the plot doesn't fully substantiate the increase in BET SSA and decreased average pore size in X-650 relative to X-RT (Fig. 6a). However, DFT model showed larger volume of smaller pores in X-650, relative to X-RT. Figures 6c and d plot the comparative PSD of X-RT and X-650 splits, derived using DFT model. DFT method, unlike BJH adsorption model, takes into account the effect of adsorption potential on location of pore condensation transition and thereby is more suitable for characterizing narrow mesopores using nitrogen adsorption, which is generally underestimated in the BJH adsorption model (Chandra and Vishal 2020; Pang et al. 2021). In Fig. 6c, it can be clearly seen that the volume of pores [dV/dlog(D)] till 4 nm width is larger than in X-650, relative to X-RT. Similarly, the cumulative volume of pores at the narrow mesopores ranges in X-650 is manifolds higher than that is X-RT (Fig. 6d), although the overall pore volume is lower. This substantiates the higher BET SSA and lower pore size of X-650, relative to X-RT.

3.2.2 Changes in fractal dimensions due to thermal treatment

Frenkel – Halsey – Hill (FHH) fractal model was used for determining the fractal dimensions of the shales and to understand the evolution of pore complexities as thermal treatment temperatures increased. The details and how the FHH model is used to calculate fractal dimensions (D) are presented in Yang et al. (2014) and Li et al. (2016). In general, fractal dimensions are recognized to be of two types-D1 and D2. Smaller mesopores (2 to 8 nm diameter) gets saturated inside the relative pressure stretch of 0.01 to 0.5 and the behaviour here is controlled by the Van der Waals forces; fractal dimensions calculated in this domain is represented as D1. On the other hand, larger mesopores (> 8 nm to 50 nm diameter) are saturated in the relative pressure range of 0.5 to 0.99 through the mechanism of capillary condensation; fractal dimensions calculated in this domain is represented as D1. For both the set of shale samples used in this study, significant alterations in fractal dimensions was noted with changing thermal treatment temperatures (Table 2).

The FHH plots of the two shales and the thermally treated counterparts are presented in Figs. 7 and 8. For sample X-RT and its splits, in general, fractal dimension D2 was observed to show better correlation with other pore properties (viz. BET SSA and average pore diameter; Fig. 9A and B). D1 and D2 first exhibited a decline from 2.40 to 2.75, respectively (in the case of X-RT), to 2.24 and 2.67 (for X-350). While D2 was observed to fall further for X-500 (2.61), D1 showed substantial increase (2.44). For split X-650, similar to other pore properties, both D1 and D2 showed sharp increase (2.78 and 2.93, respectively), indicating formation of complex porous structures owing to thermal treatment. For the other set of samples (Y series), the changes in fractal dimensions with changing temperatures of treatment were observed to be non-systematic and slightly complex, with D2 showing good correlation with other pore parameters and D1 showing little or no correlation (Figs. 9c and d). Y-RT showed the highest fractal dimensions indicating presence of complex porous structures. A reduction in both D1 and D2 was noted for Y-350, followed by a subsequent decrease in D2 and an increase in D1 for Y-500. For the Y-650 split, while D2 was observed to increase, D1 was observed to be lower than Y-500. The non-systematic variations in the evolution of fractal dimensions of both sets of shale samples used in this study, indicates certain complexities in understanding their pore structural attributes. This could be attributed to closure of preexisting pores with increased temperatures of treatment or restricted entry of nitrogen into the smaller pores, thereby producing non-systematic variations. It is also important to consider that, low pressure nitrogen gas adsorption presents certain challenges, especially when considered for evaluating pore structures in organic-rich rocks, especially for those with TOC > 10 wt% (Hazra et al. 2020). Previous research works focused on coals by several (viz. Gan et al. (1972), Parkash and Chakrabartty (1986), Mahajan (1984, 1991), Mastalerz

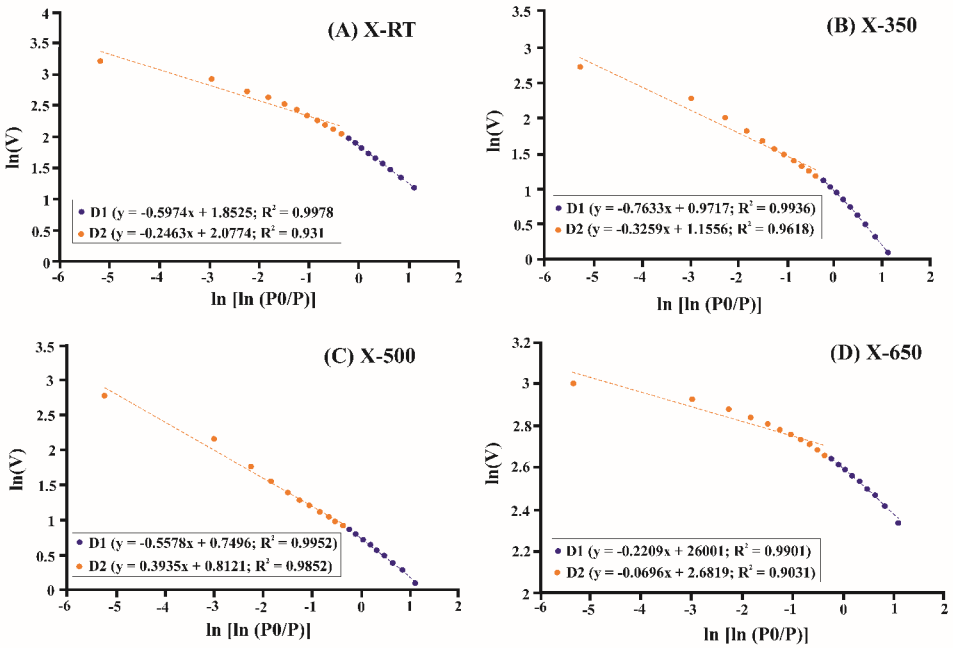

Fig. 7 Fractal plots of sample **a** X-RT shale and its thermally treated counterparts: **b** X-350, **c** X-500, and **d** X-650

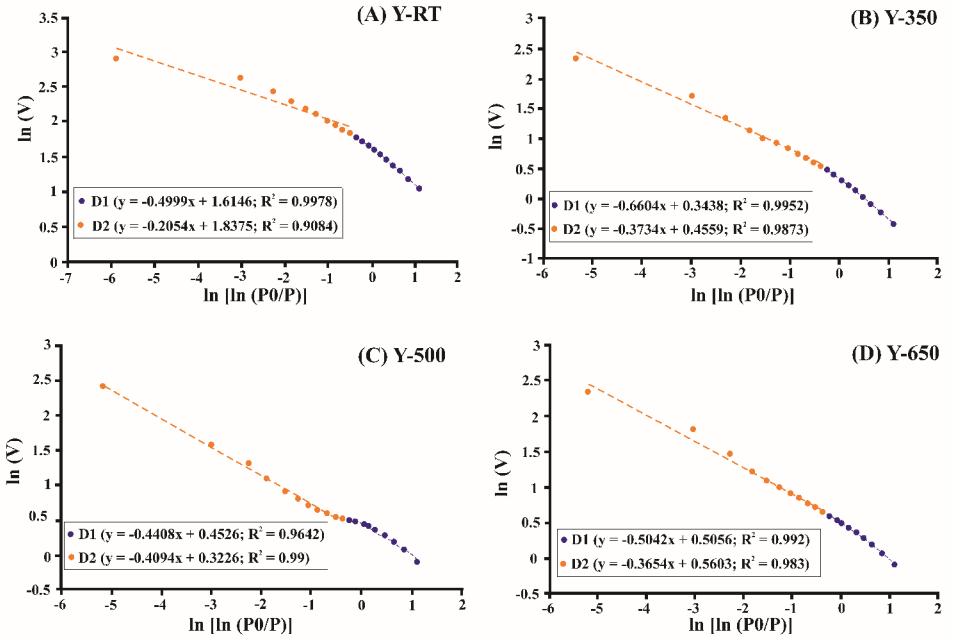

Fig. 8 Fractal plots of sample **a** Y-RT shale and its thermally treated counterparts: **b** Y-350, **c** Y-500, and **d** Y-650

et al. (2009) and Okolo et al. (2015)) have revealed very low N_2 gas adsorption derived SSA of coals, while the same samples when analysed using CO_2 as the adsorbent revealed very high micropore surface areas. It may be argued that the data from N_2 and CO_2 should not be compared as essentially different pore structures (mesopores vs. micropores) are assessed by the two adsorbents, however, the decreased N_2 adsorption derived surface areas for coals and organic-rich rocks (TOC > 10 wt%) is somewhat counter-intuitive (Hazra et al. 2020). Moreover, N_2 due to its low kinetic energy at -196 °C experimental temperatures present challenges in accessing/penetrating intricate pore structures in coals and also due to potential shrinkage of pores at such low experimental temperatures (Anderson et al. 1962; Walker et al. 1988; Mahajan 1991). Additionally, coaly organic matter is also known to have molecular sieve properties with large number of pores being lower than equal to 4 Å, which limits entry of N_2 at -196 °C, but allows passage of CO_2 (Lamond 1962; Thomas and Damberger 1976; Mahajan and Walker 1978). The shales used in this study are marked by higher

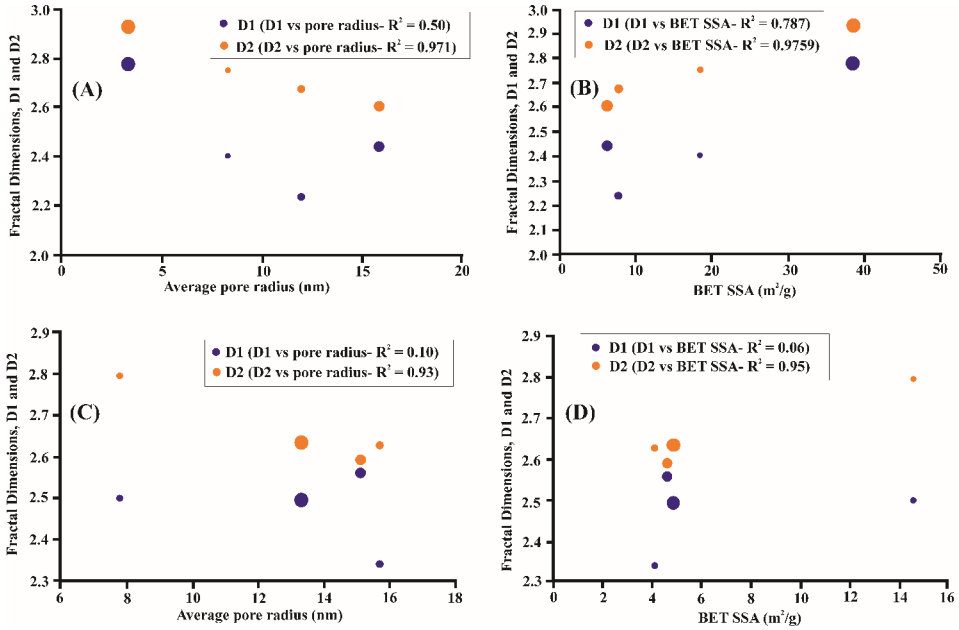

Fig. 9 Cross-plots illustrating relationship between fractal dimensions, D1 and D2 with other pore properties for the X-series (**a** and **b**) and Y-series (**c** and **d**) of samples. Note: The increasing sizes of the sample symbols corresponds to increasing thermal treatment temperatures

Table 3 Pore structural parameters obtained through low-pressure CO_2 gas adsorption

No.	D – *R* micropore surface area (m^2/g)	D – *R* micropore volume (cc/g)	D – *R* pore width (nm)	D – A micropore volume (cc/g)	D – A pore diameter (nm)	DFT surface area (m^2/g)	DFT pore volume (cc/g)
X-RT	49.554	0.019	0.866	0.025	1.360	49.442	0.015
X-350	45.920	0.017	0.850	0.021	1.340	46.064	0.014
X-500	67.042	0.025	0.787	0.024	1.260	70.974	0.020
X-650	80.891	0.030	0.761	0.028	1.240	88.669	0.024
Y-RT	71.226	0.027	0.842	0.033	1.320	70.475	0.021
Y-350	61.873	0.023	0.831	0.025	1.300	61.976	0.018
Y-500	92.359	0.035	0.770	0.032	1.240	101.140	0.028
Y-650	100.468	0.038	0.749	0.037	1.220	111.475	0.030

TOC content (16.46 wt% and 28.98 wt%), and are collected from the coal-bearing Barakar Formation of Rajmahal basin. Previous study in this area indicates the predominance of type III-IV kerogen within the shales (Sethi et al. 2023). For the studied thermally stimulated organic-rich shales, it is entirely possible that certain sieving effect is imparted by the coaly organic matter, resulting in reduction in surface areas with increasing temperatures of treatment. Similarly, the variable and non-systematic variations of fractal dimensions, especially D1 (representing the smaller mesopores (2 to 8 nm diameter) within the relative pressure stretch of 0.01 to 0.5) also indicates certain complexities, which might be related to the lack of assessment of porous structures formed due to thermal stimulation by the N_2 at the experimental conditions. Comparison of the data produced from N_2 with that of CO_2 would indicate whether the non-uniform variation generated are related to the pore properties of the shales or due to limitations of N_2 in accessing some of the pore structures.

3.3 Inferences from low pressure CO_2 gas adsorption

Low-pressure CO_2 adsorption experiments were conducted on both the raw shales and the thermally stimulated counterparts to investigate the changes in micropore properties of the samples, with changing temperatures of treatment. The findings from the low-pressure CO_2 adsorption are presented in Table 3. The isotherms, overall, can be categorized as Type I, indicating a greater adsorption rate at lower relative pressures. Sample Y-RT, marked by higher TOC content, was observed to show higher adsorption capacity, surface area, pore volume and reduced pore size in comparison to X-RT. This observation suggests the existence of larger volumes of micropores within the organic-rich sample. This is opposite to the observation from N_2 adsorption, where higher surface area and pore volume was observed in sample X-RT, relative to Y-RT. When both the samples were thermally treated at 350 °C, some drop in CO_2 uptake capacity was noted (Fig. 10). Although a similar drop in N_2 adsorption derived mesopore properties was also noted,

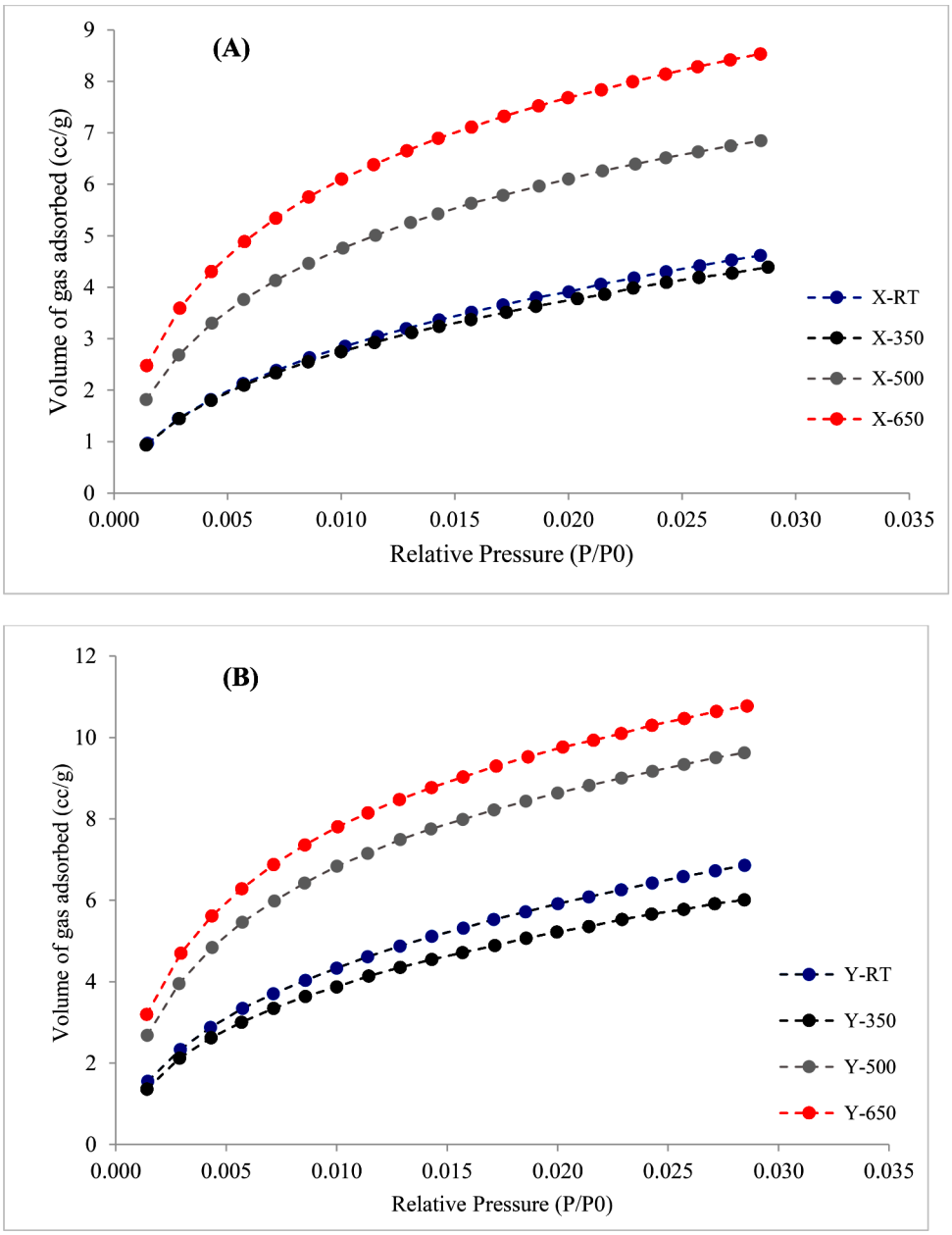

Fig. 10 Low-pressure CO_2 gas adsorption isotherms of the **a** X series and **b** Y series samples used in this study

however, the decrease from CO_2 adsorption was observed to be less sharp. Nevertheless, this indicates closure of some of the micropores that were present within the raw samples due to thermal treatment at 350 °C. Micropore size distributions calculated using the CO_2-based DFT model further corroborated these findings (Fig. 11).Compared to X-RT for the X-350 split, till ~0.45 nm pore width, new additional openings can be noted; however, beyond that the volume of pores in the X-350 split can be observed to be substantially lower than the X-RT split (Fig. 11). For Y-350, the volume of pores was noted to be lower than that of Y-RT, thereby indicating closure of some pores (Fig. 11).

Opposite to what was observed from N_2 adsorption, from CO_2 adsorption a sharp increase in CO_2 uptake capacity was observed for X-500 (~1.5 times higher than X-RT) and Y-500 (~1.4 times higher than Y-RT). Similarly, for these splits, micropore surface areas was observed to sharply increase (higher than the raw splits). This increase on CO_2 micropore surface area, CO_2 uptake capacity for the X-500 and Y-500 splits, indicates significant formation of micropores owing to thermal treatment at 500 °C, which is also corroborated from the micropore size distributions (Fig. 11). For the splits treated at 650 °C, the micropore surface areas and micropore volumes were observed to further increase, indicating formation of newer micropores due to thermal treatment at 650 °C. Micropore size distributions plots also revealed formation of greater volume of pores in X-650 and R-650, compared to X-500 and Y-500. Overall, the results

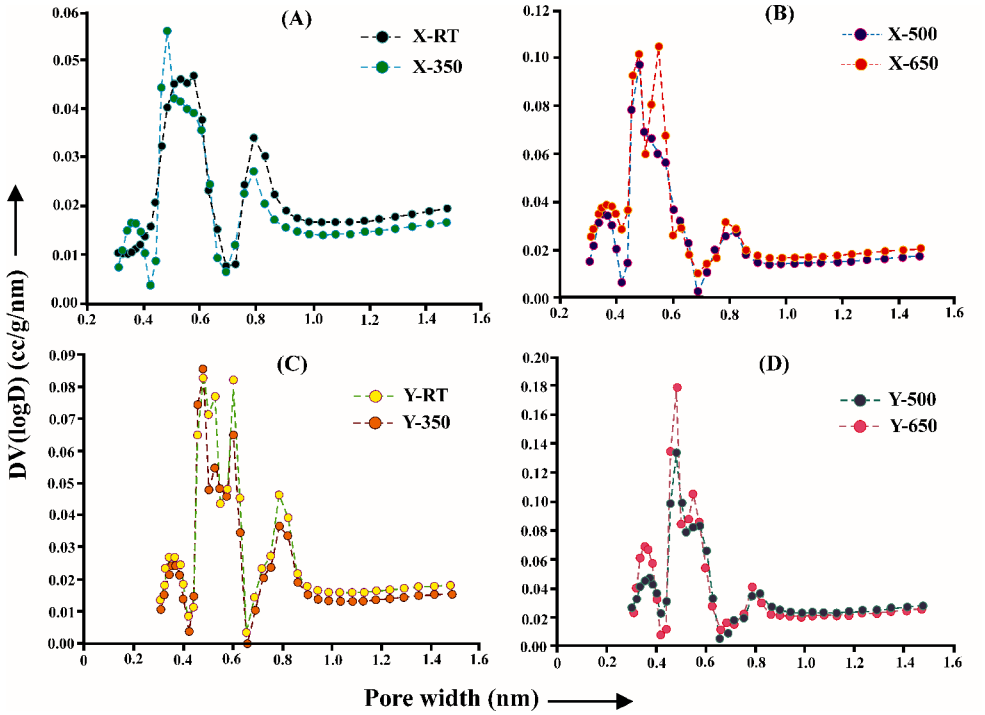

Fig. 11 Micropore size distributions for the X series (**a** and **b**) and Y series (**c** and **d**) samples calculated using the CO_2-based DFT model

from CO_2 adsorption in a way contradicts the findings from N_2 gas adsorption which may be indicative of the limitations of N_2 in accessing complex pore structures formed in the organic-rich samples owing to thermal treatment.

3.4 Implications from electron microscopy

Generally, observations from Scanning Electron Microscopy or Imaging do not actually validate or substantiate the pore properties derived from low pressure gas adsorption. The target of conducting Scanning Electron Microscopy of the thermally treated shales was not to correlate the observations from SEM with low pressure gas adsorption, but to independently examine the impact of thermal treatment on SEM observable porosity. It is fairly well established that as thermal maturity of organic matter in sedimentary rocks increase, microporosity (< 2 nm) increases and the importance of macroporosity is diminished (Okolo et al. 2015; Mastalerz et al., 2018). Previous research has documented that SEM observations can only probe/image pores with diameters ≥ 2 nm (i.e., meso- and macro-pores) (Liu et al., 2017; Mastalerz et al., 2018), and micropores (< 2 nm) which plays the most important role is adsorption of gases (both for unconventional gas production and CO_2 sequestration) are not identifiable under SEM. Consequently, comparison/correlation of porosity determined from SEM with that of other methods such as low pressure gas adsorption is largely uncertain and likewise the legitimacy of any calculation of storage capacity based on SEM-identifiable porosity is largely doubtful (İnan et al., 2018).

The SEM images of the two shale samples and their thermally treated counterparts show interesting evolution in pore structure. X-RT shows microcracks in OM matrix (Figs. 12a, b). Pore size in X-RT have a modal average of 182 nm with a maximum pore size of 2 µm. Pores are elongated with a high aspect ratio and are primarily hosted within the organic matter. Both pores and microcracks serve as gas adsorption sites. X-350 shows elongated lenticular pores similar to X-RT (Figs. 12c, d), however the opening of the pores are wider and has lower aspect ratio compared to pores in X-RT, suggesting that thermal treatment opens up the pre-existing pores. After further thermal treatment at 500 °C, the X-500 shale shows more circular pores (Figs. 12e, f), i.e., pores with lower aspect ratio as compared to X-RT and X-350. No newly formed pores were found within the scanned region, however the increase in width of the existing pores results in increase in volume of the existing pores. After further heating at 650 °C, the X-650 shale shows interesting evidence of pore collapse (Figs. 12g, h). Pre-existing pores separated by thin layer of organic matter gets ruptured and two or more pores merge to form a bigger pore. The orange circle in Fig. 12h indicate evidences of rupture of pore wall between multiple pores, which was not seen in lesser thermally treated shales. Aside from merging of pores, some distortion of the organic matrix is observed in some cases, indicating possibility of new pore formation or dilation of extremely small pores; however, the resolution of SEM images was unable to conclusively indicate that.

Similar to X-RT, Y-RT also shows numerous microcracks and elongated pores in the organic matrix and clay minerals

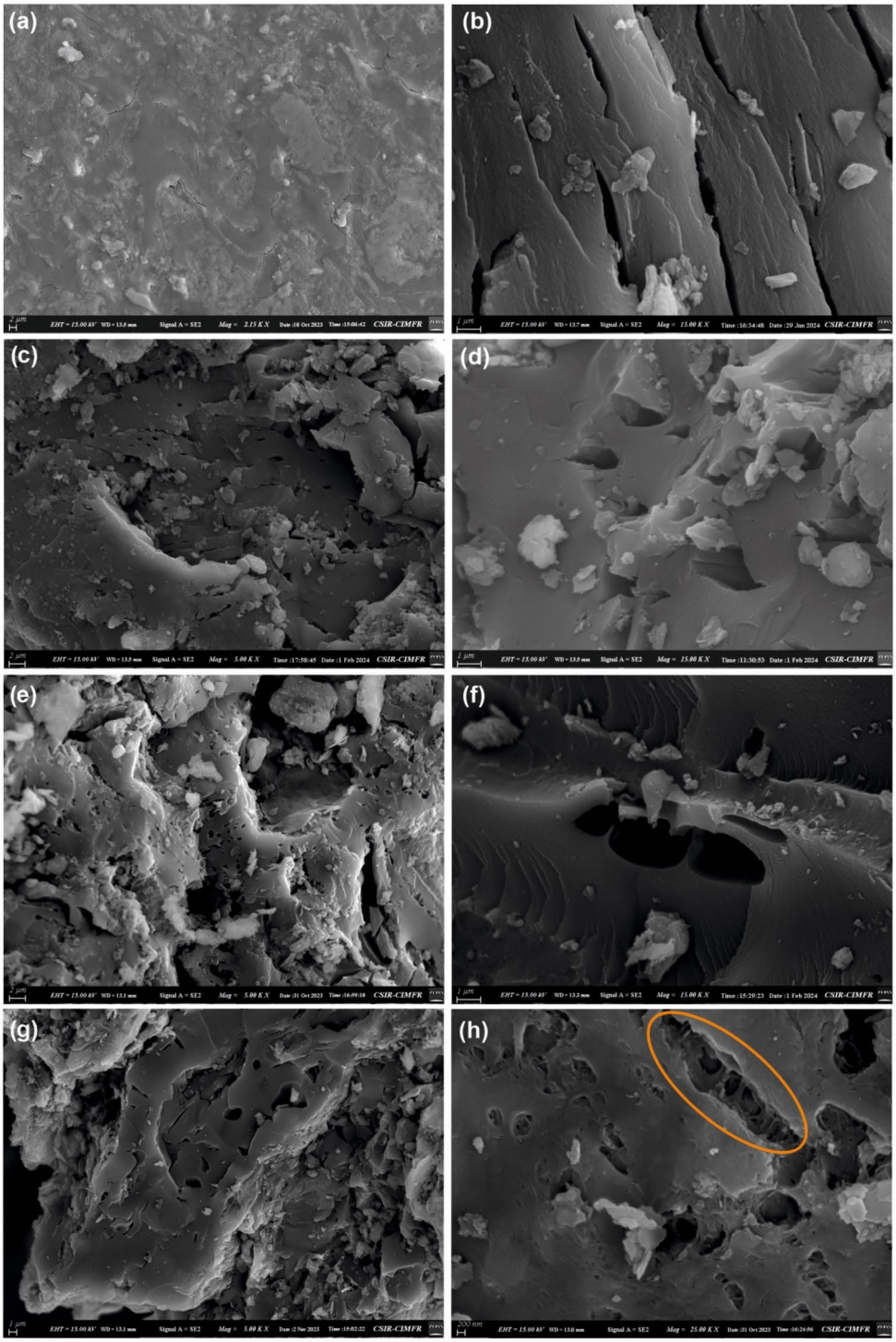

Fig. 12 SEM images of shale X (**a**, **b**)- X-RT untreated (**c**, **d**)- X-350 after 350 °C thermal treatment (**e**, **f**)- X-500 after 500 °C thermal treatment and (**g**, **h**)- X-650 after 650 °C thermal treatment. The marked area (**h**) represents signatures of pores merging due to thermal treatment

(Figs. 13a, b). There are abundant mesopores with a modal average width of 300 nm based on the SEM images of different magnification taken at various spots of the visible surface. Similar to shale X, shale Y also shows elongated pores with higher aspect ratio at lower temperatures which starts dilating along the short axis with increasing temperature (Figs. 13c, d). Unlike X, the pore dilation between 350 °C (Y-350) (Figs. 13c, d) and 500 °C (Y-500) (Figs. 13e, f) is apparently insignificant. Y-650 (Figs. 13g, h) shows circular pores with smoother pore walls as seen in X-650, however there was no evidence of pore wall rupture as seen in X-650. For both X and Y, multiple images demonstrated evidence of clay mineral pores, however these pore systems didn't show significant change with increasing temperature. A summary

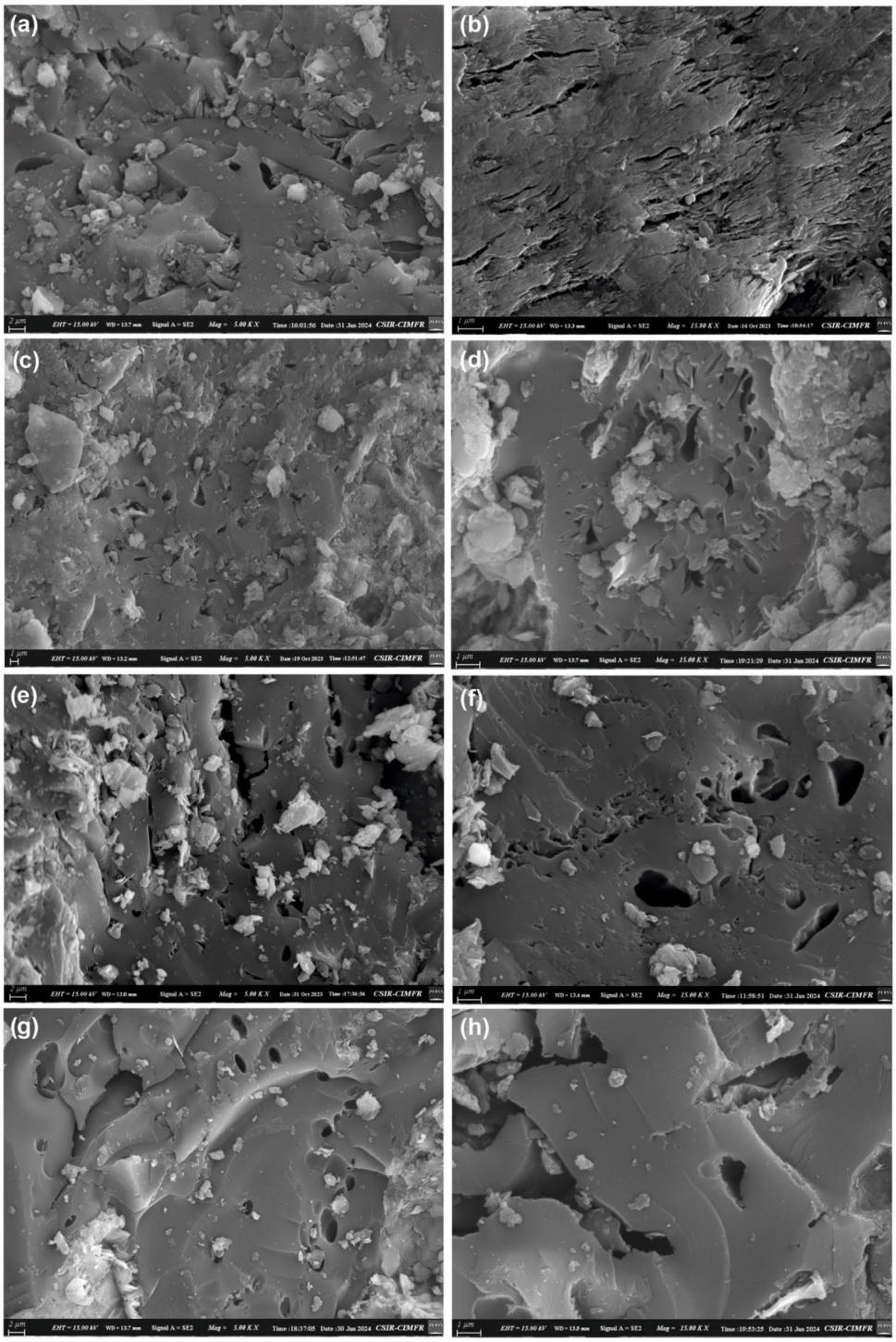

Fig. 13 SEM images of shale Y (**a**, **b**)- X-RT untreated (**c**, **d**)- X-350 after 350 °C thermal treatment (**e**, **f**)- X-500 after 500 °C thermal treatment and (**g**, **h**)- X-650 after 650 °C thermal treatment

of the pore size, aspect ratio and their change with temperature for both the shale samples are shown in Table 4.

4 Implications for in-situ thermal stimulation of shales

The results essentially indicate that owing to thermal treatment (under inert conditions), as more and more hydrocarbons are expelled from the samples, the remaining organic matter becomes more aromatized (as revealed from the Rock-Eval results), and is accompanied by formation of more micropores (as revealed from CO_2 adsorption experiments). These microporous sites, can be used for sequestrating atmospheric CO_2. Consequently, similar to underground coal thermal treatment (Zhang et al. 2017; Shi et al. 2022), if deep underground organic-rich shales are thermally stimulated, it can result is generation of cleaner hydrocarbons and also create sites for CO_2 sequestration. While, the temperature protocols used in the experiments for this study indicate that at 650 °C almost all pyrolyzable component from the kerogen is generated and the shale-char created at this temperature has maximum micropore capacity for CO_2 storage, however, depending upon the thermal maturity stage of a specific shale horizon and the type of kerogen it consists of, the temperature of in-situ pyrolysis can vary, as thermally immature shales with greater concentration of reactive kerogen start generating hydrocarbons at lower temperatures (Singh et al. 2021; Hazra et al. 2023). On the other hand, shales marked by higher thermal maturities and presence of less reactive kerogen would need higher temperatures for reacting, generating hydrocarbons and creating microporous sites for CO_2 sequestration. Thus, establishing the heating programs for in situ shale conversion should be based on the kerogen type present and the thermal maturity stage of the horizon.

In addition to alterations in shale pore structure resulting from thermal treatment, the project outcomes may also be impacted by the thermal treatment-induced propagation of fractures. The distribution and interconnection of fracture pathways within shale formations play a crucial role in the preservation, concentration, and productivity of pyrolysis byproducts (Geng et al. 2017; Li et al. 2022). When subjected to high-temperature treatment, the interconnected nanopores within the organic matter undergo enlargement, giving rise to numerous micropores and fractures, ultimately leading to increased complexity in the shale's fracture networks and a significant enhancement in the quality of the shale matrix for gas recovery and storage (Kang et al. 2016; Lei et al. 2021). Moreover, the crack pattern and thermal cracking efficiency can be notably influenced by the thermal expansion coefficients of various minerals as the thermal treatment temperature rises (Liu et al. 2020). With increasing temperatures of thermal treatment, the number and maximum aperture of fractures in shales increase (Geng et al. 2017). The fracture toughness of shale diminishes with rising in-situ temperature, while simultaneously, fracture toughness anisotropy increases; notably, fracture paths aligned with bedding orientations of 0°, 30°, and 90° exhibit minimal sensitivity to temperature variations, whereas those with 45° and 60° bedding orientations are affected (Guo et al. 2023). In general, the heat induced fracture development in shale result in reduced strength and elastic properties, (Vishal et al. 2022; Zheng et al. 2023). Thus, a number of other factors viz. geomechanical stability of the thermally stimulated horizon, propagation of fractures, impact of supercritical phase transition of sequestered CO_2 (SC-CO_2) and its interaction with thermally stimulated shales etc., can influence the outcomes for such projects, and future studies directed in these areas can help in targeting underground organic-rich shales for extraction of cleaner hydrocarbons and sequestration of atmospheric CO_2.

5 Conclusions

(1) The results from low pressure N_2 gas adsorption experiments were observed to be in contradiction to the results when CO_2 was used as the adsorbent. This could be attributed to the relative inability of N_2 to access complex structures formed in the thermally treated splits.
(2) With rising thermal treatment temperatures, micropore surface area and volume, were first noted to decrease (by ~ 7% and 13%, at 350 °C), followed by sharp increase (by ~ 30% to 35% at 500 °C and ~ 41% to 63% at 650 °C), for both the samples, compared to the raw samples, indicating formation of new micropores and thereby increasing the sequestration potential.
(3) Results from Rock-Eval indicate that for the shales used in this study, at 650 °C almost the entire pyrolyzable component of the kerogen is liberated. Additionally, the maximum micropore capacity determined from CO_2 gas adsorption experiments for these splits indicate 650 °C to be the best temperature for in situ conversion and CO_2 sequestration. However, other factors viz.

Table 4 Summary of the observed variations in pore properties through FE-SEM

Properties	X-RT	X-350	X-500	X-650	Y-RT	Y-350	Y-500	Y-650
Avg. pore width (short axis) (nm)	92	285	351	644	72	336	382	878
Aspect ratio	8–25	6–10	4–6	1–3	14–30	8–12	7–8	2–3

geomechanical stability of the treated horizon, SC-CO_2-shale interaction should be considered for such projects.

(4) The FESEM imaging of the two shales and their heated counterparts reveal that the average pore width and pore aspect ratio consistently increases and decreases respectively and with temperature. When comparing untreated and 650 °C heated counterparts, sample X and Y show 11x and 29x increase in pore width respectively. This is accompanied by a reduction in aspect ratio by 8x and 10x for sample X and Y respectively. This indicates that the newly formed pores are not only bigger, but also appear more circular on visible surface.

Abbreviations

HF	Hydraulic fracturing
UCTT	Underground coal thermal treatment
TOC	Total organic carbon
FE-SEM	Field emission scanning electron microscope
LPGA	Low pressure gas adsorption
BJH	Barret-Joyner-Halenda
PSD	Pore size distribution
BET	Brunauer, Emmett and Teller
DA	Dubinin-Astakhov
DR	Dubinin-Radushkevich
DFT	Density functional theory
HHH	Frenkel-Halsey-Hill
SSA	Specific surface area
SE2	Secondary Electron
A_sB	Angle Selective Backscattered
PC	Pyrolyzable carbon
RC	Residual carbon
HI	Hydrogen index
OI	Oxygen index

Supplementary Information The online version contains supplementary material available at https://doi.org/10.1007/s40789-024-00717-6.

Acknowledgements The Director CSIR-CIMFR is thankfully acknowledged for giving permission and for providing necessary infrastructure to conduct this research. B Hazra thankfully acknowledges the Science and Engineering Research Board, Department of Science and Technology, Government of India for the SERB International Research Experience award for the year 2023–2024 (Award Number: SIR/2022/001610).

Author contributions Bodhisatwa Hazra: Conceptualisation of manuscript, Interpretation of results, Writing- original draft. Debanjan Chandra: Interpretation of results, Writing- review & editing. Vikram Vishal: Writing- review & editing. Mehdi Ostadhassan: Checking and upgradation of the quality of the manuscript, interpretation of results. Chinmay Sethi: Execution of experiments, preparation of figures and tables. Binoy Kumar Saikia: Checking and upgradation of the quality of the manuscript, Supervision. Jai Krishna Pandey: Checking and upgradation of the quality of the manuscript, Supervision. Atul K Varma: Checking and upgradation of the quality of the manuscript.

Funding This study did not receive any external funds.

Data availability Data will be made available on request.

Declarations

Conflict of interest The authors declare that they have no known competing financial interests or personal relationships that could have appeared to influence the work reported in this paper.

References

Anderson RB, Hofer LJ, Bayer J (1962) Surface area of coal. Fuel; (United Kingdom) 41:559

Bai F, Sun Y, Liu Y, Guo M (2017) Evaluation of the porous structure of Huadian oil shale during pyrolysis using multiple approaches. Fuel 187:1–8. https://doi.org/10.1016/j.fuel.2016.09.012

Bao X, Eaton DW (2016) Fault activation by hydraulic fracturing in western Canada. Science 354(6318):1406–1409. https://doi.org/10.1126/science.aag2583

Chandra D, Vishal V (2020) A comparison of nano-scale pore attributes of Barakar formation gas shales from Raniganj and Wardha Basin, India using low pressure sorption and FEG-SEM analysis. J Nat Gas Sci Eng 81:103453. https://doi.org/10.1016/j.jngse.2020.103453

Barrett EP, Joyner LG, Halenda PP (1951) The determination of pore volume and area distributions in porous substances. I. Computations from nitrogen isotherms. J AM Chem 73(1):373–380.

Chandra D, Bakshi T, Vishal V (2021) Thermal effect on pore characteristics of shale under inert and oxic environments: insights on pore evolution. Microporous Mesoporous Mater 316:110969. https://doi.org/10.1016/j.micromeso.2021.110969

Chandra D, Vishal V, Bahadur J, Agrawal AK, Das A, Hazra B, Sen D (2022) Nano-scale physicochemical attributes and their impact on pore heterogeneity in shale. Fuel 314:123070. https://doi.org/10.1016/j.fuel.2021.123070

Chandra D, Bakshi T, Bahadur J, Hazra B, Vishal V, Kumar S, Sen D, Singh TN (2023) Pore morphology in thermally-treated shales and its implication on CO_2 storage applications: a gas sorption, SEM, and small-angle scattering study. Fuel 331:125877. https://doi.org/10.1016/j.fuel.2022.125877

Chen W, Lei Y, Chen Y, Sun J (2016) Pyrolysis and combustion enhance recovery of gas for two China shale rocks. Energy Fuels 30(12):10298–10305. https://doi.org/10.1021/acs.energyfuels.6b02274

Chen W, Lei Y, Ma L, Yang L (2017) Experimental study of high temperature combustion for enhanced shale gas recovery.

Energy Fuels 31(9):10003–10010. https://doi.org/10.1021/acs.energyfuels.7b00762
Chen W, Zhou Y, Yang L, Zhao N, Lei Y (2018) Experimental study of low-temperature combustion characteristics of shale rocks. Combust Flame 194:285–295. https://doi.org/10.1016/j.combustflame.2018.04.033
Dąbrowski A (2001) Adsorption—from theory to practice. Adv Colloid Interface Sci 93(1–3):135–224. https://doi.org/10.1016/S0001-8686(00)00082-8
De Boer JH (1958) The structure and properties of porous materials. In: Proceedings of the Tenth Symposium of the Colston Research Society Held in the University of Bristol, Butterworths, London, pp. 68–94
Du F, Nojabaei B (2019) A review of gas injection in shale reservoirs: enhanced oil/gas recovery approaches and greenhouse gas control. Energies 12(12):2355. https://doi.org/10.3390/en12122355
Gan H, Nandi SP, Walker PL Jr (1972) Nature of the porosity in American coals. Fuel 51(4):272–277. https://doi.org/10.1016/0016-2361(72)90003-8
Geng Y, Liang W, Liu J, Cao M, Kang Z (2017) Evolution of pore and fracture structure of oil shale under high temperature and high pressure. Energy & Fuels. 31(10):10404–10413
Godec M, Koperna G, Petrusak R, Oudinot A (2013) Potential for enhanced gas recovery and CO2 storage in the Marcellus Shale in the Eastern United States. Int J Coal Geol 118:95–104. https://doi.org/10.1016/j.coal.2013.05.007
Günay A, Arslankaya E, Tosun I (2007) Lead removal from aqueous solution by natural and pretreated clinoptilolite: adsorption equilibrium and kinetics. J Hazard Mater 146(1–2):362–371. https://doi.org/10.1016/j.jhazmat.2006.12.034
Guo W, Zhang X, Deng S, Sun Y, Han J, Bai F, Kang S, He W (2022) Enhanced pyrolysis of Huadian oil shale at high temperature in the presence of water and air atmosphere. J Pet Sci Eng 215:110623. https://doi.org/10.1016/j.petrol.2022.110623
Hazra B, Dutta S, Kumar S (2017) TOC calculation of organic matter rich sediments using Rock-Eval pyrolysis: critical consideration and insights. Int J Coal Geol 169:106–115. https://doi.org/10.1016/j.coal.2016.11.012
Hazra B, Wood DA, Vishal V, Singh AK (2018a) Pore characteristics of distinct thermally mature shales: influence of particle size on low-pressure CO_2 and N_2 adsorption. Energy Fuels 32(8):8175–8186. https://doi.org/10.1021/acs.energyfuels.8b01439
Hazra B, Wood DA, Kumar S, Saha S, Dutta S, Kumari P, Singh AK (2018b) Fractal disposition, porosity characterization and relationships to thermal maturity for the Lower Permian Raniganj basin shales, India. J Nat Gas Sci Eng 59:452–465. https://doi.org/10.1016/j.jngse.2018.09.014
Hazra B, Karacan CÖ, Tiwari DM, Singh PK, Singh AK (2019) Insights from Rock-Eval analysis on the influence of sample weight on hydrocarbon generation from Lower Permian organic matter rich rocks, West Bokaro basin, India. Mar Pet Geol 106:160–170. https://doi.org/10.1016/j.marpetgeo.2019.05.006
Hazra B, Vishal V, Singh DP (2020) Applicability of low-pressure CO_2 and N_2 adsorption in determining pore attributes of organic-rich shales and coals. Energy Fuels 35(1):456–464. https://doi.org/10.1021/acs.energyfuels.0c03412
Hazra B, Singh DP, Chakraborty P, Singh PK, Sahu SG, Adak AK (2021) Using rock-eval S4Tpeak as thermal maturity proxy for shales. Mar Pet Geol 127:104977. https://doi.org/10.1016/j.marpetgeo.2021.104977
Hazra B, Vishal V, Sethi C, Chandra D (2022) Impact of supercritical CO_2 on shale reservoirs and its implication for CO_2 sequestration. Energy Fuels 36(17):9882–9903. https://doi.org/10.1021/acs.energyfuels.2c01894
Hazra B, Chandra D, Lahiri S, Vishal V, Sethi C, Pandey JK (2023) Pore evolution during Combustion of distinct thermally mature Shales: insights into potential. Situ Convers Energy Fuels 37(18):13898–13911. https://doi.org/10.1021/acs.energyfuels.3c02320
Heller R, Zoback M (2014) Adsorption of methane and carbon dioxide on gas shale and pure mineral samples. J Unconv Oil Gas Resour 8:14–24. https://doi.org/10.1016/j.juogr.2014.06.001
İnan S, Al Badairy H, İnan T, Al Zahrani A (2018) Formation and occurrence of organic matter-hosted porosity in shales. Int J Coal Geol 199:39–51
Jarvie DM, Hill RJ, Ruble TE, Pollastro RM (2007) Unconventional shale-gas systems: the Mississippian Barnett Shale of north-central Texas as one model for thermogenic shale-gas assessment. AAPG Bull 91(4):475–499. https://doi.org/10.1306/12190606068
Kang Y, Chen M, Chen Z, You L, Hao Z (2016) Investigation of formation heat treatment to enhance the multiscale gas transport ability of shale. Journal of Natural Gas Science and Engineering. 35:265–275
Kang Z, Zhao Y, Yang D (2020) Review of oil shale in-situ conversion technology. Appl Energy 269:115121. https://doi.org/10.1016/j.apenergy.2020.115121
Kelly KE, Wang D, Hradisky M, Silcox GD, Smith PJ, Eddings EG, Pershing DW (2016) Underground coal thermal treatment as a potential low-carbon energy source. Fuel Process Technol 144:8–19. https://doi.org/10.1016/j.fuproc.2015.12.006
Khalili NR, Pan M, Sandí G (2000) Determination of fractal dimensions of solid carbons from gas and liquid phase adsorption isotherms. Carbon 38(4):573–588
Krumm RL (2014) Carbon dioxide sequestration in in situ thermally treated coal and oil shale formations. Dissertation, The University of Utah
Kuila U, Prasad M (2013) Specific surface area and pore-size distribution in clays and shales. Geophysical Prospecting, 61(2-Rock Physics for Reservoir Exploration, Characterisation and Monitoring), 341–362
Labani MM, Rezaee R, Saeedi A, Al Hinai A (2013) Evaluation of pore size spectrum of gas shale reservoirs using low pressure nitrogen adsorption, gas expansion and mercury porosimetry: a case study from the Perth and Canning basins, Western Australia. J Petrol Sci Eng 112:7–16. https://doi.org/10.1016/j.petrol.2013.11.022
Lamond TG (1962) Ph. D. Thesis, University of Durham, England
Lei J, Pan B, Guo Y, Fan Y, Xue L, Deng S, Zhang L, Ruhan A (2021) A comprehensive analysis of the pyrolysis effects on oil shale pore structures at multiscale using different measurement methods. Energy 227:120359. https://doi.org/10.1016/j.energy.2021.120359
Li A, Ding W, He J, Dai P, Yin S, Xie F (2016) Investigation of pore structure and fractal characteristics of organic-rich shale reservoirs: a case study of Lower Cambrian Qiongzhusi formation in Malong block of eastern Yunnan Province, South China. Mar Pet Geol 70:46–57. https://doi.org/10.1016/j.marpetgeo.2015.11.004
Li Y, Xiong J, Wu G, Liu X, Liang L, Ding Y, Wu F (2022) Effect of high temperature on the physical properties and pore structure characteristics of organic-rich shale. Arab J Geosci 15(7):586. https://doi.org/10.1007/s12517-022-09867-w
Liu B, Schieber J, Mastalerz M, (2017) Combined SEM and reflected light petrography of organic matter in the New Albany Shale (Devonian-Mississippian) in the Illinois Basin: a perspective on organic pore development with thermal maturation. Int J Coal Geol 184:57–72
Liu J, Liang X, Xue Y, Yao K, Fu Y (2020) Numerical evaluation on multiphase flow and heat transfer during thermal stimulation enhanced shale gas recovery. Appl Therm Eng 178:115554. https://doi.org/10.1016/j.applthermaleng.2020.115554
Lyu Q, Tan J, Li L, Ju Y, Busch A, Wood DA, Ranjith PG, Middleton R, Shu B, Hu C, Wang Z (2021) The role of supercritical carbon dioxide for recovery of shale gas and sequestration in gas shale

reservoirs. Energy Environ Sci 14(8):4203–4227. https://doi.org/10.1039/D0EE03648J
Mahajan OP (1984) Physical characterization of coal. Powder Technol 40(1–3):1–15. https://doi.org/10.1016/0032-5910(84)85052-4
Mahajan OP (1991) CO2 surface area of coals: the 25-year paradox. Carbon 29(6):735–742. https://doi.org/10.1016/0008-6223(91)90010-G
Mahajan OP, Walker PL Jr (1978) Reactivity of heat-treated coals. Analytical methods for coal and coal products. Academic, pp 465–494
Mastalerz M, Drobniak A, Schimmelmann A (2009) Changes in optical properties, chemistry, and micropore and mesopore characteristics of bituminous coal at the contact with dikes in the Illinois Basin. Int J Coal Geol 77(3–4):310–319. https://doi.org/10.1016/j.coal.2008.05.014
Mastalerz M, Drobniak A, Stankiewicz AB (2018) Origin, properties, and implications of solid bitumen in source-rock reservoirs: a review. Int J Coal Geol 195:14–36
Okolo GN, Everson RC, Neomagus HW, Roberts MJ, Sakurovs R (2015) Comparing the porosity and surface areas of coal as measured by gas adsorption, mercury intrusion and SAXS techniques. Fuel 141:293–304. https://doi.org/10.1016/j.fuel.2014.10.046
Pang P, Han H, Hu L, Guo C, Gao Y, Xie Y (2021) The calculations of pore structure parameters from gas adsorption experiments of shales: which models are better? J Nat Gas Sci Eng 94:104060. https://doi.org/10.1016/j.jngse.2021.104060
Parkash S, Chakrabartty SK (1986) Microporosity in Alberta plains coals. Int J Coal Geol 6(1):55–70. https://doi.org/10.1016/0166-5162(86)90025-X
Peters KE, Cassa MR (1994) Applied source rock geochemistry. In: Magoon LB, Dow WG (Eds.), The Petroleum System—from Source to Trap: AAPG Memoir 60:93–120
Pirngruber G (2016) Physisorption and pore size analysis. Characterization of porous solids-characterization of catalysts and surfaces. Institut Francais du Petrole. 68 pages
Rouquerol J, Rouquerol F, Sing KSW (1998) Absorption by powders and porous solids. Academic
Sethi C, Mastalerz M, Hower JC, Hazra B, Singh AK, Vishal V (2023) Using optical-electron correlative microscopy for shales of contrasting thermal maturity. Int J Coal Geol 104273. https://doi.org/10.1016/j.coal.2023.104273
Shi Q, Cui S, Wang S, Mi Y, Sun Q, Wang S, Shi C, Yu J (2022) Experiment study on CO2 adsorption performance of thermal treated coal: inspiration for CO_2 storage after underground coal thermal treatment. Energy 254:124392. https://doi.org/10.1016/j.energy.2022.124392
Shi Y, Zhang Y, Song X, Cui Q, Lei Z, Song G (2023) Injection energy utilization efficiency and production performance of oil shale in-situ exploitation. Energy 263:125714. https://doi.org/10.1016/j.energy.2022.125714
Sing KS (1985) Reporting physisorption data for gas/solid systems with special reference to the determination of surface area and porosity (recommendations 1984). Pure Appl Chem 57(4):603–619
Singh DP, Chandra D, Vishal V, Hazra B, Sarkar P (2021) Impact of degassing time and temperature on the estimation of pore attributes in shale. Energy Fuels 35(19):15628–15641. https://doi.org/10.1021/acs.energyfuels.1c02201
Sun L, Tuo J, Zhang M, Wu C, Wang Z, Zheng Y (2015) Formation and development of the pore structure in Chang 7 member oil-shale from Ordos Basin during organic matter evolution induced by hydrous pyrolysis. Fuel 158:549–557. https://doi.org/10.1016/j.fuel.2015.05.061
Taheri-Shakib J, Kantzas A (2021) A comprehensive review of microwave application on the oil shale: prospects for shale oil production. Fuel 305:121519. https://doi.org/10.1016/j.fuel.2021.121519
Thomas J, Damberger HH (1976) Internal surface area, moisture content, and porosity of Illinois coals: variations with coal rank. Circular no. 493
Thommes M, Kaneko K, Neimark AV, Olivier JP, Rodriguez-Reinoso F, Rouquerol J, Sing KS (2015) Physisorption of gases, with special reference to the evaluation of surface area and pore size distribution (IUPAC Technical Report). Pure Appl Chem 87(9–10):1051–1069. https://doi.org/10.1515/pac-2014-1117
Tiwari P, Deo M, Lin CL, Miller JD (2013) Characterization of oil shale pore structure before and after pyrolysis by using X-ray micro CT. Fuel 107:547–554. https://doi.org/10.1016/j.fuel.2013.01.006
Vishal V, Chandra D, Bahadur J, Sen D, Hazra B, Mahanta B, Mani D (2019) Interpreting pore dimensions in gas shales using a combination of SEM imaging, small-angle neutron scattering, and low-pressure gas adsorption. Energy Fuels 33(6):4835–4848. https://doi.org/10.1021/acs.energyfuels.9b00442
Vishal V, Rizwan M, Mahanta B, Pradhan SP, Singh TN (2022) Temperature effect on the mechanical behavior of shale: Implication for shale gas production. Geosystems and Geoenvironment. 1(4):100078
Walker PL Jr, Verma SK, Rivera-Utrilla J, Khan MR (1988) A direct measurement of expansion in coals and macerais induced by carbon dioxide and methanol. Fuel 67(5):719–726. https://doi.org/10.1016/0016-2361(88)90305-5
Wang K, Li H, Wang J, Jiang B, Bu C, Zhang Q, Luo W (2017) Predicting production and estimated ultimate recoveries for shale gas wells: a new methodology approach. Appl Energy 206:1416–1431. https://doi.org/10.1016/j.apenergy.2017.09.119
Xu W, Yu H, Micheal M, Huang H, Liu H, Wu H (2023) An integrated model for fracture propagation and production performance of thermal enhanced shale gas recovery. Energy 263:125682. https://doi.org/10.1016/j.energy.2022.125682
Yang F, Ning Z, Liu H (2014) Fractal characteristics of shales from a shale gas reservoir in the Sichuan Basin, China. Fuel 115:378–384. https://doi.org/10.1016/j.fuel.2013.07.040
Yao Y, Liu D, Tang D, Tang S, Huang W (2008) Fractal characterization of adsorption-pores of coals from North China: an investigation on CH4 adsorption capacity of coals. Int J Coal Geol 73:27–42
Zhang HR, Li S, Kelly KE, Eddings EG (2017) Underground in situ coal thermal treatment for synthetic fuels production. PECS 62:1–32. https://doi.org/10.1016/j.pecs.2017.05.003
Zhang P, Lu S, Li J, Wang J, Zhang J, Yin Y (2023) Pore structure characterizations of Shale Oil reservoirs with Heat Treatment: a Case Study from Dongying Sag, Bohai Bay Basin, China. ACS Omega 8(29):26508–26525. https://doi.org/10.1021/acsomega.3c03260
Zheng Y, Jia C, Zhang S, Shi C (2023) Experimental and constitutive modeling of the anisotropic mechanical properties of shale subjected to thermal treatment. Geomech Energy Environ 35:100485
Zhuoke L, Lin T, Liu X, Ma S, Li X, Yang F, He B, Liu J, Zhang Y, Xie L (2023) High-Temperature-Induced Pore System Evolution of Immature Shale with different total Organic Carbon contents. ACS Omega 8(14):12773–12786. https://doi.org/10.1021/acsomega.2c07990

Authors and Affiliations

Bodhisatwa Hazra[1,2] · Debanjan Chandra[3] · Vikram Vishal[4,5] · Mehdi Ostadhassan[2] · Chinmay Sethi[1] · Binoy K. Saikia[6] · Jai Krishna Pandey[1] · Atul K. Varma[7]

✉ Bodhisatwa Hazra
bodhisatwa.hazra@gmail.com

[1] CSIR- Central Institute of Mining and Fuel Research, Dhanbad, Jharkhand 826001, India

[2] Institute of Geosciences, Marine and Land Geomechanics and Geotectonics, Christian- Albrechts-Universität, 24118 Kiel, Germany

[3] Department of Geoscience and Engineering, Delft University of Technology, Delft 2628 CN, The Netherlands

[4] Computational and Experimental Geomechanics Laboratory, Department of Earth Sciences, Indian Institute of Technology (IIT) Bombay, Mumbai 400076, India

[5] National Centre of Excellence in Carbon Capture and Utilization, Indian Institute of Technology (IIT) Bombay, Mumbai 400076, India

[6] Coal & Energy Group, CSIR North-East Institute of Science & Technology, Jorhat 785006, India

[7] Department of Applied Geology, Indian Institute of Technology (Indian School of Mines), Dhanbad, Jharkhand 826004, India